

Torsional Oscillations of Relativistic Stars with Dipole Magnetic Fields II. Global Alfvén Modes

H. Sotani^{*}, K. D. Kokkotas[†], N. Stergioulas[‡], and M. Vavoulidis[§]

Department of Physics, Aristotle University of Thessaloniki, Thessaloniki 54124, Greece

14 August 2018

ABSTRACT

We investigate torsional Alfvén modes of relativistic stars with a global dipole magnetic field. It has been noted recently (Glampedakis et al. 2006) that such oscillation modes could serve as an alternative explanation (in contrast to torsional crustal modes) for the SGR phenomenon, if the magnetic field is not confined to the crust. We compute global Alfvén modes for a representative sample of equations of state and magnetar masses, in the ideal MHD approximation and ignoring $\ell \pm 2$ terms in the eigenfunction. We find that the presence of a realistic crust has a negligible effect on Alfvén modes for $B > 4 \times 10^{15}$ G. Furthermore, we find strong avoided crossings between torsional Alfvén modes and torsional crust modes. For magnetar-like magnetic field strengths, the spacing between consecutive Alfvén modes is of the same order as the gap of avoided crossings. As a result, it is not possible to identify modes of predominantly crustal character and all oscillations are predominantly Alfvén-like. Interestingly, we find excellent agreement between our computed frequencies and observed frequencies in two SGRs, for a maximum magnetic field strength in the range of $(0.8\text{--}1.2) \times 10^{16}$ G.

Key words: relativity – MHD – stars: neutron – stars: oscillations – stars: magnetic fields – gamma rays: theory

1 INTRODUCTION

Soft Gamma Repeaters (SGRs) have attracted a lot of attention recently, since there exist at least two sources in which quasi-periodic oscillations have been observed. The frequency of these oscillations, in the tail of the burst, indicate that they must originate in the vicinity of the SGR source, thought to be a magnetar (Duncan & Thompson 1992). A popular model for explaining these oscillations involves the excitation of torsional modes in the solid crust of the star (Duncan 1998). An alternative explanation has been provided by Glampedakis et al. (2006). In a simple toy model, they showed that, in addition to crustal modes, a magnetized star could also have a discrete spectrum of global Alfvén modes, which would dominate over crustal modes for sufficiently strong magnetic fields. Here we investigate global, torsional Alfvén modes in realistic models of relativistic stars with a global dipole magnetic field and compare our computed frequencies with observations.

SGRs produce giant flares with peak luminosities of $10^{44} - 10^{46}$ erg/s, which display a decaying tail for several hundred seconds. Up to now, three giant flares have been detected, SGR 0526-66 in 1979, SGR 1900+14 in 1998, and SGR 1086-20 in 2004. The timing analysis of the latter two events revealed several quasi-periodic oscillations (QPOs) in the decaying tail, with frequencies of 18, 26, 29, 92.5, 150, 626.5, and 1837 Hz for SGR 1806-20 and 28, 54, 84, and 155 Hz for SGR 1900+14 (see Strohmayer & Watts (2006) and references therein). Furthermore, for SGR 1806-20 the possible detection of two additional higher frequencies (720 Hz and 2384 Hz) has been reported (Strohmayer & Watts 2006).

Spherical stars have generally two type oscillations, spheroidal modes with even parity and the toroidal modes with axial

^{*} E-mail: sotani@astro.auth.gr

[†] E-mail: kokkotas@auth.gr

[‡] E-mail: niksterg@astro.auth.gr

[§] E-mail: miltos@astro.auth.gr

parity. The observed QPOs in SGR tails are thought to originate from toroidal oscillations, since the latter are excited more easily than poloidal oscillations, as toroidal modes do not involve density variations. In Newtonian theory, there have been several investigations of torsional modes in neutron star crusts, see e.g. Hansen & Cioffi (1980); McDermott et al. (1988); Carroll et al. (1986); Strohmayer (1991); Lee (2006). On the other hand, only a few studies have taken general relativity into account Schumaker & Thorne (1983); Leins (1994); Messios et al. (2001); Sotani et al. (2006); Samuelsson & Andersson (2006). The more recent of these studies (see e.g. Sotani et al. (2006), hereafter Paper I) have shown that some of the observational data of SGRs could agree with the crust torsional modes, if, e.g., frequencies lower than 155 Hz are identified with the fundamental modes of different harmonic index ℓ , while higher frequencies are identified with overtones. However, as mentioned in Paper I it will be quite challenging to identify all observed QPO frequencies with crustal torsional modes. For example, it is difficult to explain both the frequencies of 26 and 29 Hz for SGR 1806-20 for a single stellar model, because the actual spacing of torsional modes of the crust is larger than the difference between these two frequencies. Similarly, the spacing between the 626.5 and 720 Hz QPOs in SGR 1806-20 may be too small to be explained by consecutive overtones of crustal torsional modes. In the present paper, we show that such difficulties are avoided if one identifies the observed frequencies with global Alfvén modes.

The article is structured as follows: in the next section 2 we briefly summarize the equations to be solved and the assumptions made. In section 3 we discuss the numerical results, where to understand qualitatively the properties of global Alfvén modes we also treat two special cases. The comparison with the observed data in SGRs are done in section 4 and finally we give a summary and discussion in section 5. Unless otherwise noted, we adopt units of $c = G = 1$, where c and G denote the speed of light and the gravitational constant, respectively, while the metric signature is $(-, +, +, +)$.

2 MAIN EQUATIONS AND NUMERICAL METHOD

The main equations and numerical method required for the present study have already been derived in Paper I. Here, we only give a brief summary of the main assumptions and final relations.

We assume that the equilibrium stellar model is described by a solution of the TOV equations for nonrotating, relativistic stars and a metric of the form

$$ds^2 = -e^{2\Phi} dt^2 + e^{2\Lambda} dr^2 + r^2(d\theta^2 + \sin^2\theta d\phi^2), \quad (1)$$

where Φ and Λ are functions of the Schwarzschild radial coordinate r . We neglect the influence of the magnetic field on the equilibrium configuration, since the magnetic energy $\mathcal{E}_{\mathcal{M}}$ is negligible, compared to the gravitational binding energy $\mathcal{E}_{\mathcal{G}}$, $\mathcal{E}_{\mathcal{M}}/\mathcal{E}_{\mathcal{G}} \approx 10^{-4}(B/(10^{16}G))^2$.

Adopting the ideal MHD approximation, we assume that the star is endowed with a dipolar magnetic field, described by

$$H_r = \frac{e^\Lambda \cos\theta}{\sqrt{\pi}r^2} a_1, \quad (2)$$

$$H_\theta = -\frac{e^{-\Lambda} \sin\theta}{\sqrt{4\pi}} a_{1,r}. \quad (3)$$

where $H_\mu \equiv B_\mu/\sqrt{4\pi}$, with B_μ the magnetic field 4-vector, and a_1 being a function describing the radial behavior of the magnetic field. In the exterior of the star

$$a_1^{(\text{ex})} = -\frac{3\mu_b}{8M^3} r^2 \left[\ln\left(1 - \frac{2M}{r}\right) + \frac{2M}{r} + \frac{2M^2}{r^2} \right], \quad (4)$$

where μ_b is the magnetic dipole moment for an observer at infinity (Wasserman & Shapiro 1983), while the interior solution is found by solving Maxwell's equations for the ϕ -component of the electromagnetic 4-potential A_μ , assuming a particular form for the 4-current J_ϕ (Konno et al. 1999).

We have used a variety of neutron star models, using four different equations of state for the core, ranging from a very soft EoS (EoS A) (Pandharipande 1971) to a very stiff (EoS L) (Pandharipande & Smith 1975), with two intermediate ones, EoS WFF3 (Wiringa et al. 1988) and APR (Akmal et al. 1998). For each EoS we constructed a number of models, starting from a gravitational mass of $1.4M_\odot$ and reaching close to the maximum mass limit in increments of $0.2M_\odot$. In order to separately investigate the effect of the composition of the crust, we matched the various high-density EoS to two different proposed equations of state for the crust, one recent derived by Douchin & Haensel (2001) (DH) and, for reference, and older EoS by Negele & Vautherin (1973) (NV). The two crust EoS differ significantly both in the detailed composition, as well as in the density at the base of the crust, which is at $\rho \approx 2.4 \times 10^{14} \text{ gr/cm}^3$ for Negele & Vautherin (1973) and at $\rho \approx 1.28 \times 10^{14} \text{ gr/cm}^3$ for Douchin & Haensel (2001). For the stiff EoS these different properties of the crust have a considerable effect on the bulk properties. Figure 1 of Paper I displays the mass-radius relationship of nonrotating equilibrium models constructed with the various high-density EoS, in combination with our two choices for the crust EoS. The individual models for which we compute torsional modes are shown with symbols, while their detailed properties are also listed in Table 1 of Paper I.

For studying individual oscillation modes, the linearized dynamical equations governing the magnetized fluid and crust are specialized to the case of axial perturbations, adopting the relativistic Cowling approximation (i.e. neglecting spacetime perturbations). In this case, the only nonvanishing perturbed fluid variable is (assuming a harmonic time dependence with frequency ω)

$$\delta u^\phi = i\omega e^{-\Phi} \mathcal{Y}(r) e^{i\omega t} b(\theta), \quad (5)$$

where

$$b(\theta) \equiv \frac{1}{\sin\theta} \partial_\theta P_\ell(\cos\theta), \quad (6)$$

and ∂_θ denotes the partial derivative with respect to θ . Above, $\mathcal{Y}(r)$ describes the radial dependence of the angular displacement of the stellar material, $P_\ell(\cos\theta)$ is the Legendre polynomial of order ℓ and we have set $m = 0$, due to the degeneracy in m for a spherically symmetric background.

The linearized induction equation in the MHD approximation relates the perturbation in the magnetic field to $\mathcal{Y}(r)$. Neglecting magnetic-field-induced $\ell \pm 2$ couplings leads to the eigenvalue equation

$$\begin{aligned} \left[\mu + (1 + 2\lambda_1) \frac{a_1^2}{\pi r^4} \right] \mathcal{Y}'' &+ \left\{ \left(\frac{4}{r} + \Phi' - \Lambda' \right) \mu + \mu' + (1 + 2\lambda_1) \frac{a_1}{\pi r^4} [(\Phi' - \Lambda') a_1 + 2a_1'] \right\} \mathcal{Y}' \\ &+ \left\{ \left[\left(\epsilon + p + (1 + 2\lambda_1) \frac{a_1^2}{\pi r^4} \right) e^{2\Lambda} - \frac{\lambda_1 a_1'^2}{2\pi r^2} \right] \omega^2 e^{-2\Phi} \right. \\ &\quad \left. - (\lambda - 2) \left(\frac{\mu e^{2\Lambda}}{r^2} - \frac{\lambda_1 a_1'^2}{2\pi r^4} \right) + (2 + 5\lambda_1) \frac{a_1}{2\pi r^4} \{ (\Phi' - \Lambda') a_1' + a_1'' \} \right\} \mathcal{Y} = 0, \end{aligned} \quad (7)$$

where μ is the shear modulus in the crust and

$$\lambda = \ell(\ell + 1), \quad (8)$$

$$\lambda_1 = -\frac{\ell(\ell + 1)}{(2\ell - 1)(2\ell + 3)}. \quad (9)$$

In order to solve a system of first-order ODEs, we define new variables \mathcal{Y}_1 and \mathcal{Y}_2 , through

$$\mathcal{Y}_1 \equiv \mathcal{Y} r^{1-\ell}, \quad (10)$$

$$\mathcal{Y}_2 \equiv \left[\mu + (1 + 2\lambda_1) \frac{a_1^2}{\pi r^4} \right] e^{\Phi-\Lambda} \mathcal{Y}' r^{2-\ell}. \quad (11)$$

In defining the new variables, we took into account the form of the eigenfunction \mathcal{Y} near the center, where $\mathcal{Y} \sim r^{\ell-1}$. The final first-order system of equations to be solved numerically for the real eigenvalues ω is then

$$\mathcal{Y}_1' = -\frac{\ell-1}{r} \mathcal{Y}_1 + \frac{\pi r^3}{\pi r^4 \mu + (1 + 2\lambda_1) a_1^2} e^{-\Phi+\Lambda} \mathcal{Y}_2, \quad (12)$$

$$\begin{aligned} \mathcal{Y}_2' = & - \left[\left(\epsilon + p + (1 + 2\lambda_1) \frac{a_1^2}{\pi r^4} - \lambda_1 e^{-2\Lambda} \frac{a_1'^2}{2\pi r^2} \right) \omega^2 r e^{2(\Lambda-\Phi)} \right. \\ & \left. - (\lambda - 2) \left(\frac{\mu e^{2\Lambda}}{r} - \frac{\lambda_1 a_1'^2}{2\pi r^3} \right) + (2 + 5\lambda_1) \frac{a_1 e^{2\Lambda}}{\pi r^3} \left(\frac{a_1}{r^2} - 2\pi j_1 \right) \right] e^{\Phi-\Lambda} \mathcal{Y}_1 - \frac{\ell+2}{r} \mathcal{Y}_2, \end{aligned} \quad (13)$$

where the unperturbed Maxwell's equations were used in order to eliminate the term of a_1'' .

The above system of equations is solved as an eigenvalue problem, imposing a) regularity at the center, b) a continuous traction condition at the crust-core interface, and c) a zero-torque condition at the stellar surface. Regularity at the center implies

$$\mathcal{Y}_2 = (\ell - 1) \left[\mu + (1 + 2\lambda_1) \frac{\alpha_c^2}{\pi} \right] e^\Phi \mathcal{Y}_1. \quad (14)$$

The demand that the traction is continuous at the crust-core interface implies

$$\mathcal{Y}'^{(-)} = \left[1 + \frac{1}{1 + 2\lambda_1} \frac{u_s^2}{u_A^2} \right] \mathcal{Y}'^{(+)}. \quad (15)$$

where u_s and u_A are the shear and Alfvén velocities, respectively. With our choice of variables, this condition becomes $\mathcal{Y}_2^{(-)} = \mathcal{Y}_2^{(+)}$. At the stellar surface, the zero-torque condition $\delta T_\phi^{(s)r} = 0$ (Schumaker & Thorne 1983) implies $\mathcal{Y}_2 = 0$. We neglect the possible presence of a thin fluid ocean.

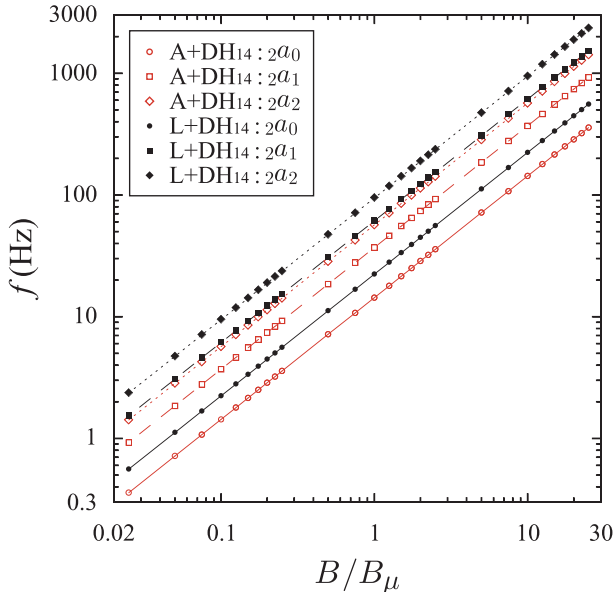


Figure 1. Frequencies of Alfvén modes, ${}_{\ell}a_n$, with $\ell = 2$ and $n = 0, 1$, and 2 as a function of the normalized magnetic field B/B_{μ} . The equilibrium models have mass $1.4M_{\odot}$ and only results for a very soft (A) and a very stiff (L) high-density EOS are shown, combined with the DH EOS for the crust (see text). Individual numerical results are shown with various marks, while the continuous lines correspond to the empirical formula (17) with coefficient values in shown in Tables 1, 2, and 3.

Specific frequencies of predominantly or pure crustal modes are labeled as ${}_{\ell}t_n$, while the frequencies of predominantly or pure Alfvén modes are labeled as ${}_{\ell}a_n$, where ℓ is the angular index and n is associated with the number of radial nodes in the eigenfunction of various overtones.

3 NUMERICAL RESULTS

Our equilibrium models comprise both a fluid part and a thin solid crust, which can have a thickness ranging from about 3% to 12% of the stellar radius, depending on the EOS and mass. We will compute global torsional Alfvén modes in the presence of both of these components. However, in order to understand qualitatively the properties of these modes, we will first study them in the limiting case where one neglects the presence of a solid crust and treats the model as a pure magneto-fluid. In addition, in order to understand the influence of the presence of a solid crust on the Alfvén modes (and, conversely, the influence of a global magneto-fluid on the torsional crust modes) we will study a toy model of varying crust thickness, before focusing on the realistic models presented in the previous section.

3.1 Global Alfvén modes for a pure magneto-fluid

As a limiting case, we first consider global Alfvén modes, in the absence of a solid crust, i.e. setting $\mu = 0$ in the crust region. These modes are pure Alfvén modes and degenerate to zero frequency in the limit of a vanishing magnetic field, since then the eigenvalue problem becomes

$$(\epsilon + p)e^{-2\Phi+2\Lambda}\omega^2\mathcal{Y} = 0, \quad (16)$$

which has $\omega = 0$ as a trivial solution. In the presence of a magnetic field, the eigenfrequency becomes proportional to the magnetic field strength B .

Figure 1 shows the frequency of several modes (with $\ell = 2$ and $n = 0, 1, 2$) as a function of the strength of the magnetic field, for $1.4M_{\odot}$ models of a very soft (A) and a very stiff (L) EOS. Various lines in the figure are linear fits to the numerical data. As is apparent from these numerical results, the linearity of the frequency as a function of B is preserved to a very high accuracy, at least in the range of $B = 10^{14} - 10^{17}$ G. Therefore, our numerical results can be represented by the following empirical formula

$${}_{\ell}a_n = {}_{\ell}\beta_n \left(\frac{B}{B_{\mu}} \right), \quad (17)$$

Table 1. The values for the fitting factors ${}_{\ell}\beta_0$ (Hz) of equation (17). The fitting factors have been calculated for magnetic field strengths up to 10^{17} G.

Model	$2\beta_0$	$3\beta_0$	$4\beta_0$	$5\beta_0$	$6\beta_0$	$7\beta_0$	$8\beta_0$
A+DH ₁₄	14.32	17.67	20.28	22.66	24.91	27.08	29.18
A+DH ₁₆	10.83	13.41	15.47	17.34	19.12	20.83	22.48
WFF3+DH ₁₄	16.81	20.70	23.73	26.46	29.06	31.55	33.97
WFF3+DH ₁₆	13.85	17.08	19.61	21.90	24.08	26.18	28.21
WFF3+DH ₁₈	10.73	13.29	15.32	17.18	18.95	20.65	22.29
APR+DH ₁₄	19.17	23.62	27.06	30.16	33.10	35.93	38.67
APR+DH ₁₆	16.34	20.14	23.09	25.76	28.29	30.73	33.09
APR+DH ₁₈	13.94	17.20	19.74	22.04	24.23	26.34	28.38
APR+DH ₂₀	11.79	14.57	16.75	18.74	20.63	22.45	24.21
APR+DH ₂₂	9.70	12.03	13.54	15.55	17.16	18.70	20.19
L+DH ₁₄	22.33	27.44	31.36	34.87	38.19	41.38	44.48
L+DH ₁₆	19.58	24.04	27.47	30.54	33.44	36.24	38.95
L+DH ₁₈	17.29	21.22	24.24	26.96	29.53	32.01	34.42
L+DH ₂₀	15.29	18.77	21.45	23.87	26.15	28.36	30.52
L+DH ₂₂	13.48	16.57	18.95	21.10	23.14	25.12	27.04
L+DH ₂₄	11.78	14.50	16.60	18.52	20.34	22.10	23.81
L+DH ₂₆	9.97	12.31	14.14	15.82	17.42	18.96	20.46
A+NV ₁₄	14.26	17.59	20.19	22.55	24.79	26.95	29.03
A+NV ₁₆	10.79	13.37	15.41	17.27	19.04	20.75	22.39
WFF3+NV ₁₄	16.78	20.67	23.68	26.41	29.00	31.49	33.90
WFF3+NV ₁₆	13.83	17.06	19.58	21.87	24.05	26.14	28.17
WFF3+NV ₁₈	10.72	13.28	15.31	17.16	18.93	20.63	22.26
APR+NV ₁₄	18.47	22.72	26.00	28.95	31.74	34.43	37.04
APR+NV ₁₆	15.81	19.46	22.28	24.82	27.23	29.56	31.82
APR+NV ₁₈	13.55	16.69	19.12	21.33	23.43	25.45	27.41
APR+NV ₂₀	11.50	14.19	16.30	18.21	20.03	21.78	23.48
APR+NV ₂₂	9.49	11.76	13.54	15.17	16.72	18.22	19.67
L+NV ₁₄	20.17	24.82	28.40	31.60	34.62	37.52	40.33
L+NV ₁₆	17.72	21.80	24.92	27.71	30.35	32.89	35.36
L+NV ₁₈	15.69	19.27	22.02	24.48	26.81	29.06	31.24
L+NV ₂₀	13.91	17.08	19.51	21.69	23.76	25.75	27.70
L+NV ₂₂	12.32	15.12	17.27	19.21	21.04	22.82	24.56
L+NV ₂₄	10.81	13.27	15.17	16.88	18.52	20.10	21.64
L+NV ₂₆	9.15	11.27	12.92	14.42	15.86	17.24	18.59

where B_μ is a typical magnetic field strength, which we take to be $B_\mu = 4 \times 10^{15}$ G (as in Paper I) and ${}_{\ell}\beta_n$ are coefficients, which depend on the equilibrium model and the mode in question. For each equilibrium stellar model the coefficients ${}_{\ell}\beta_n$ for $\ell = 2 - 8$ and $n = 0, 1, 2$ are shown in Tables 1, 2, and 3.

As a general trend, one sees that the value of the coefficients ${}_{\ell}\beta_n$ becomes larger (and thus the dependence of the mode frequency on the magnetic field strength becomes stronger), as the mass of the star increases (for a given EOS). The same trend holds with increasing stiffness of the EOS, for a given mass. One also sees from the Table 1 that ${}_{\ell}\beta_0/2\beta_0 \approx \sqrt{\ell/2}$, so that the following empirical formula holds for the fundamental modes

$${}_{\ell}a_0 \approx 2\beta_0 \sqrt{\frac{\ell}{2}} \left(\frac{B}{B_\mu} \right). \quad (18)$$

Examining more closely the dependence of the mode frequency on the parameters of the equilibrium models, we find that the coefficients ${}_{\ell}\beta_0$ are a linear function of the inverse of the compactness M/R (see Figure 2), so that the frequency of the fundamental modes is approximately given by

$${}_{\ell}a_0 \approx \sqrt{\frac{\ell}{2}} \left[3.69 \left(\frac{R}{M} \right) - 3.22 \right] \left(\frac{B}{B_\mu} \right), \quad (19)$$

(with an accuracy of a few per cent). For given strength of the magnetic field the frequency of the fundamental modes varies by a factor of up to 2.4 within the set equilibrium models in Table 1. Similarly, the frequency of the $n = 1$ and $n = 2$ overtones of the $\ell = 2$ mode varies by up to a factor of 2.7. It follows that the frequency of global Alfvén modes is sensitive to the magnetic field strength and the bulk properties of the equilibrium model and a successful identification of several modes

Table 2. The values for the fitting factors ${}_{\ell}\beta_1$ (Hz) of equation (17). The fitting factors have been calculated for magnetic field strengths up to 10^{17} G.

Model	$2\beta_1$	$3\beta_1$	$4\beta_1$	$5\beta_1$	$6\beta_1$	$7\beta_1$	$8\beta_1$
A+DH ₁₄	37.02	42.91	47.26	50.94	54.24	57.28	60.15
A+DH ₁₆	26.71	31.06	34.30	37.08	39.59	41.92	44.14
WFF3+DH ₁₄	44.50	51.45	56.54	60.83	64.65	68.17	71.48
WFF3+DH ₁₆	35.80	41.48	45.67	49.22	52.39	55.32	58.08
WFF3+DH ₁₈	26.46	30.79	34.04	36.81	39.32	41.65	43.87
APR+DH ₁₄	51.63	59.53	65.28	70.12	74.42	78.39	82.11
APR+DH ₁₆	43.51	50.27	55.21	59.37	63.09	66.51	69.73
APR+DH ₁₈	36.56	42.32	46.55	50.13	53.34	56.30	59.09
APR+DH ₂₀	30.30	35.15	38.74	41.79	44.53	47.07	49.47
APR+DH ₂₂	24.18	28.14	30.43	33.63	35.92	38.05	40.08
L+DH ₁₄	61.38	70.83	77.71	83.48	88.60	93.29	97.66
L+DH ₁₆	53.30	61.56	67.57	72.61	77.08	81.17	84.99
L+DH ₁₈	46.51	53.78	59.08	63.53	67.47	71.08	74.45
L+DH ₂₀	40.55	46.93	51.61	55.54	59.03	62.23	65.22
L+DH ₂₂	35.18	40.74	44.84	48.29	51.36	54.19	56.84
L+DH ₂₄	30.13	34.93	38.47	41.46	44.14	46.61	48.94
L+DH ₂₆	24.75	28.77	31.75	34.29	36.57	38.69	40.70
A+NV ₁₄	36.88	42.75	47.07	50.74	54.02	57.05	59.90
A+NV ₁₆	26.62	30.95	34.19	36.95	39.45	41.77	43.98
WFF3+NV ₁₄	44.43	51.37	56.45	60.73	64.55	68.06	71.36
WFF3+NV ₁₆	35.77	41.44	45.63	49.16	52.33	55.26	58.02
WFF3+NV ₁₈	26.43	30.76	34.00	36.77	39.27	41.60	43.82
APR+NV ₁₄	49.79	57.43	63.00	67.66	71.81	75.61	79.18
APR+NV ₁₆	42.12	48.66	53.44	57.46	61.04	64.33	67.42
APR+NV ₁₈	35.53	41.13	45.23	48.70	51.79	54.64	57.32
APR+NV ₂₀	29.56	34.29	37.78	40.74	43.39	45.85	48.16
APR+NV ₂₂	23.68	27.54	30.43	32.90	35.13	37.20	39.16
L+NV ₁₄	56.55	65.42	71.91	77.35	82.18	86.59	90.69
L+NV ₁₆	49.07	56.88	62.60	67.40	71.65	75.52	79.12
L+NV ₁₈	42.73	49.61	54.67	58.92	62.69	66.13	69.32
L+NV ₂₀	37.20	43.21	47.65	51.40	54.73	57.77	60.60
L+NV ₂₂	32.28	37.50	41.36	44.62	47.52	50.18	52.67
L+NV ₂₄	27.68	32.15	35.45	38.25	40.75	43.05	45.20
L+NV ₂₆	22.68	26.39	29.15	31.49	33.58	35.52	37.34

would, in principle, allow the inference of both the magnetic field and the compactness of the star, through empirical relations such as Equation (19).

Figure 3 shows the frequencies with $\ell = 2, 3$, and 4 , and $n = 0, 1$, and 2 as a function of the magnetic field strength B/B_μ , for the particular stellar model A+DH₁₄. The Figure demonstrates that the frequencies of overtones depend on the value of ℓ , in sharp contrast to the case of pure crust modes, where the frequencies of overtones are almost independent of ℓ (see, e.g. Paper I).

3.2 Avoided crossings between global Alfvén modes and torsional modes of the crust

How does the presence of a solid crust affect the global Alfvén modes? And, conversely, how are the torsional modes of the crust affected when global Alfvén modes are also present? In order to answer these questions, we construct a toy model in which we introduce a crust of varying thickness $\Delta r/R$. We focus on an equilibrium models with $M = 1.4M_\odot$ and $R = 10.4$ km, constructed with a relativistic polytropic EOS with polytropic index $N = 1.0$ and polytropic constant $K = 130$ km². In this toy model, the shear modulus is simply taken to be $\mu = \rho v_s^2$, where $v_s = 1.0 \times 10^8$ cm/s (Schumaker & Thorne 1983).

If one assumes that the whole star is solid ($\Delta r/R = 1.0$) then the frequency spectrum of torsional modes only consist of crust modes. Qualitatively, the dependence of the mode frequencies on the strength of the magnetic field is similar to the results in Paper I, i.e. there is a weak dependence up to $B/B_\mu \sim 1$ (nearly horizontal branch), followed by a rapid increase in frequency for larger magnetic field strengths (magnetic-field-dominated branch). When the crust thickness is reduced to $\Delta r/R < 1$, global Alfvén modes are introduced. In such a composite fluid/crust case, the eigenfunctions of torsional crust modes penetrate inside the fluid region, i.e. crust modes become global modes and, conversely, the eigenfunctions of Alfvén modes penetrate the inside crust region. Thus, the allowed discrete global modes are only those for which the eigenfunction

Table 3. The values for the fitting factors $\ell\beta_2$ (Hz) of equation (17). The fitting factors have been calculated for magnetic field strengths up to 10^{17} G.

Model	$2\beta_2$	$3\beta_2$	$4\beta_2$	$5\beta_2$	$6\beta_2$	$7\beta_2$	$8\beta_2$
A+DH ₁₄	56.74	64.60	70.36	75.22	79.55	83.50	87.16
A+DH ₁₆	40.47	46.17	50.39	53.96	57.16	60.10	62.83
WFF3+DH ₁₄	68.12	77.39	84.13	89.80	94.82	99.40	103.64
WFF3+DH ₁₆	54.59	62.10	67.60	72.23	76.34	80.10	83.59
WFF3+DH ₁₈	40.06	45.70	49.88	53.44	56.61	59.53	62.25
APR+DH ₁₄	78.92	89.48	97.12	103.52	109.19	114.35	119.14
APR+DH ₁₆	66.42	75.38	81.87	87.32	92.14	96.54	100.62
APR+DH ₁₈	55.73	63.33	68.87	73.53	77.67	81.44	84.95
APR+DH ₂₀	46.07	52.45	57.13	61.08	64.60	67.81	70.81
APR+DH ₂₂	36.59	41.75	44.62	48.82	51.73	54.40	56.89
L+DH ₁₄	94.61	107.36	116.59	124.31	131.13	137.33	143.05
L+DH ₁₆	81.89	93.02	101.10	107.86	113.83	119.25	124.25
L+DH ₁₈	71.30	81.00	88.07	94.02	99.28	104.06	108.48
L+DH ₂₀	62.13	70.60	76.76	81.95	86.55	90.74	94.62
L+DH ₂₂	53.86	61.24	66.62	71.15	75.15	78.81	82.19
L+DH ₂₄	46.01	52.38	57.03	60.96	64.44	67.61	70.56
L+DH ₂₆	37.48	42.79	46.71	50.03	52.98	55.68	58.18
A+NV ₁₄	56.53	64.35	70.09	74.93	79.24	83.17	86.82
A+NV ₁₆	40.34	46.02	50.22	53.78	56.97	59.89	62.61
WFF3+NV ₁₄	68.02	77.27	84.00	89.66	94.67	99.24	103.47
WFF3+NV ₁₆	54.54	62.04	67.53	72.16	76.26	80.02	83.50
WFF3+NV ₁₈	40.01	45.65	49.83	53.38	56.55	59.46	62.19
APR+NV ₁₄	76.27	86.53	93.97	100.20	105.72	110.74	115.39
APR+NV ₁₆	64.38	73.09	79.41	84.71	89.40	93.66	97.62
APR+NV ₁₈	54.21	61.61	67.01	71.54	75.56	79.22	82.62
APR+NV ₂₀	44.97	51.19	55.76	59.61	63.03	66.16	69.07
APR+NV ₂₂	35.84	40.88	44.62	47.80	50.63	53.23	55.66
L+NV ₁₄	86.88	98.86	107.60	114.91	121.37	127.24	132.65
L+NV ₁₆	75.15	85.56	93.22	99.69	105.43	110.64	115.46
L+NV ₁₈	65.52	74.55	81.18	86.81	91.82	96.40	100.65
L+NV ₂₀	57.20	65.09	70.87	75.75	80.08	84.05	87.73
L+NV ₂₂	49.67	56.58	61.64	65.91	69.69	73.13	76.33
L+NV ₂₄	42.46	48.42	52.80	56.50	59.79	62.78	65.55
L+NV ₂₆	34.41	39.34	43.01	46.11	48.87	51.39	53.73

at the crust/core interface satisfies the continuous traction condition (15) exactly. As we will see, this strict requirement leads to avoided crossings between the two families of modes and to a dramatic change of the mode spectrum in the limit of small crust thickness and high magnetic field.

Figure 4 shows the first six frequencies for $\ell = 2$, as a function of the strength of magnetic field, for four different values of the crust thickness, $\Delta r/R = 0.95, 0.70, 0.50$, and 0.30 . As seen Figure 4(a) even a small fluid part ($\Delta r/R = 0.95$) allows both families of modes to be present, e.g. for small magnetic field strengths one can see both horizontal mode sequences (dashed lines, corresponding to crust modes) and Alfvén-like sequences (continuous lines). However, as the functional dependence of the global Alfvén modes with increasing magnetic field strength is different than the functional dependence of crust modes, the two families of modes appear to cross each other. On closer examination, one sees that, in fact, avoided crossings take place. For ($\Delta r/R = 0.95$) the gap at avoided crossings is still small, so that both families of modes are clearly visible. In addition, since the fluid region is still small, the Alfvén mode frequencies are high and the avoided crossings take place on the horizontal branch of the crust modes.

When the crust thickness is reduced to $\Delta r/R = 0.70$, Figure 4(b), the enlargement of the fluid region leads to a reduction of the Alfvén mode frequencies. This leads to the avoided crossings taking place at larger values of the magnetic field. The avoided crossing of the fundamental mode takes place close to the transition of the crust modes from the horizontal branch to the magnetic-field-dominated branch. Thus, a horizontal branch of predominantly crust modes is still present. However, the avoided crossings of higher-order overtones take place at the magnetic-field-dominated branch of crust modes. This leads to a significant increase in the gap at avoided crossings and one cannot easily distinguish modes that are predominantly crust modes.

Reducing the crust thickness further to $\Delta r/R = 0.50$ and 0.30 , Figures 4(c),(d), one observes that the avoided crossings of low-order modes take place in the magnetic-field-dominated branch of crust modes and the gap in avoided crossings tends

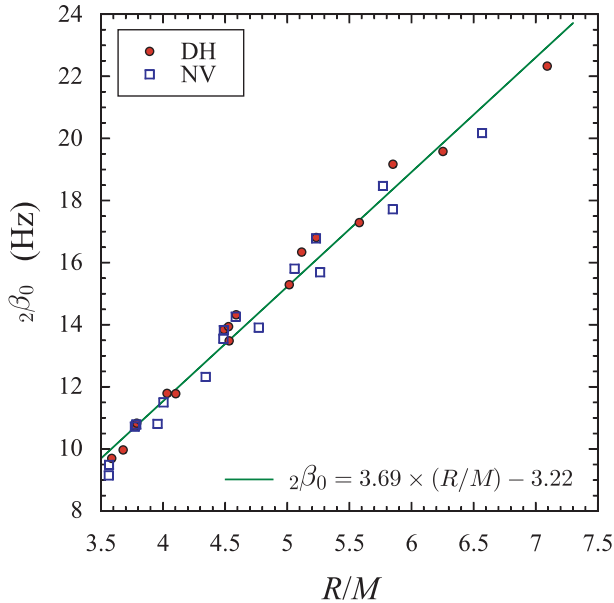


Figure 2. Distribution of the coefficients ${}_2\beta_0$ in Table 1 with respect to the inverse of stellar compactness M/R . The marks of circle and square correspond to the crust EOS DH and NV, respectively, while the solid line is a linear fit, used in constructing Equation (19).

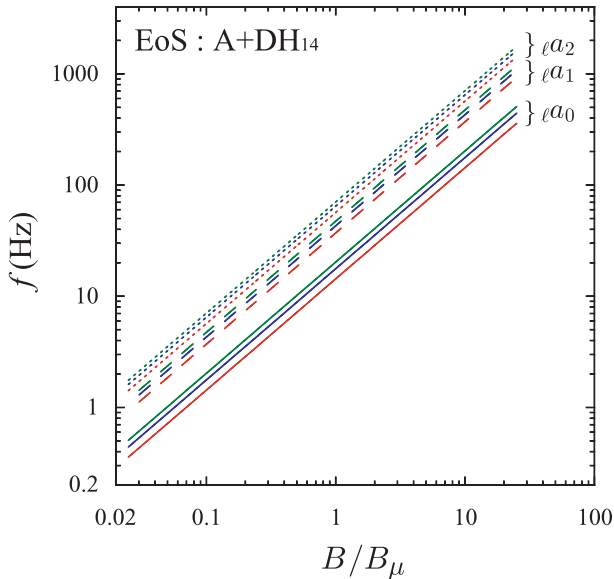


Figure 3. The frequencies of Alfvén modes for ${}_\ell a_n$ with $\ell = 2, 3$, and 4 and $n = 0, 1$, and 2 as functions of the normalized magnetic field B/B_μ . The solid, dashed, and short-dashed lines correspond to the frequencies of ${}_\ell a_0$, ${}_\ell a_1$, and ${}_\ell a_2$, respectively, and for each n the frequencies increase with increasing ℓ . For a given ℓ , the frequency of various overtones does not coincide, in sharp contrast with crustal torsional modes. The mass of the equilibrium model, constructed with the A+DH EOS, is $M = 1.4M_\odot$.

to become of the same order as the frequency spacing of consecutive Alfvén modes. The avoided crossings are now visible as only a small local change in the slope of mode-sequences, where one would expect a crust mode to be present. However, modes of predominantly crustal character are no longer distinguishable. The same trend continues when the crust thickness is reduced even further, so that for realistic values of the crust thickness (3%-12%) the mode spectrum is similar to the pure Alfvén mode spectrum shown in Figure 3.

Regarding the eigenfunctions of oscillation modes, at a given magnetic field strength, the lowest-frequency mode corresponds to a fundamental mode without any node, while the number of nodes is increasing for overtones of higher frequency. We find that the position of nodes change at avoided crossings. The inset in Figure 4(b) follows the continuous sequence of mode frequencies, which start out as the ${}_2 a_1$ Alfvén mode (first filled circle at $B/B_\mu = 0.1$). After an avoided crossing, the sequence becomes a fundamental torsional mode, ${}_2 t_0$, (second filled circle at $B/B_\mu = 0.2$). After a second avoided crossing

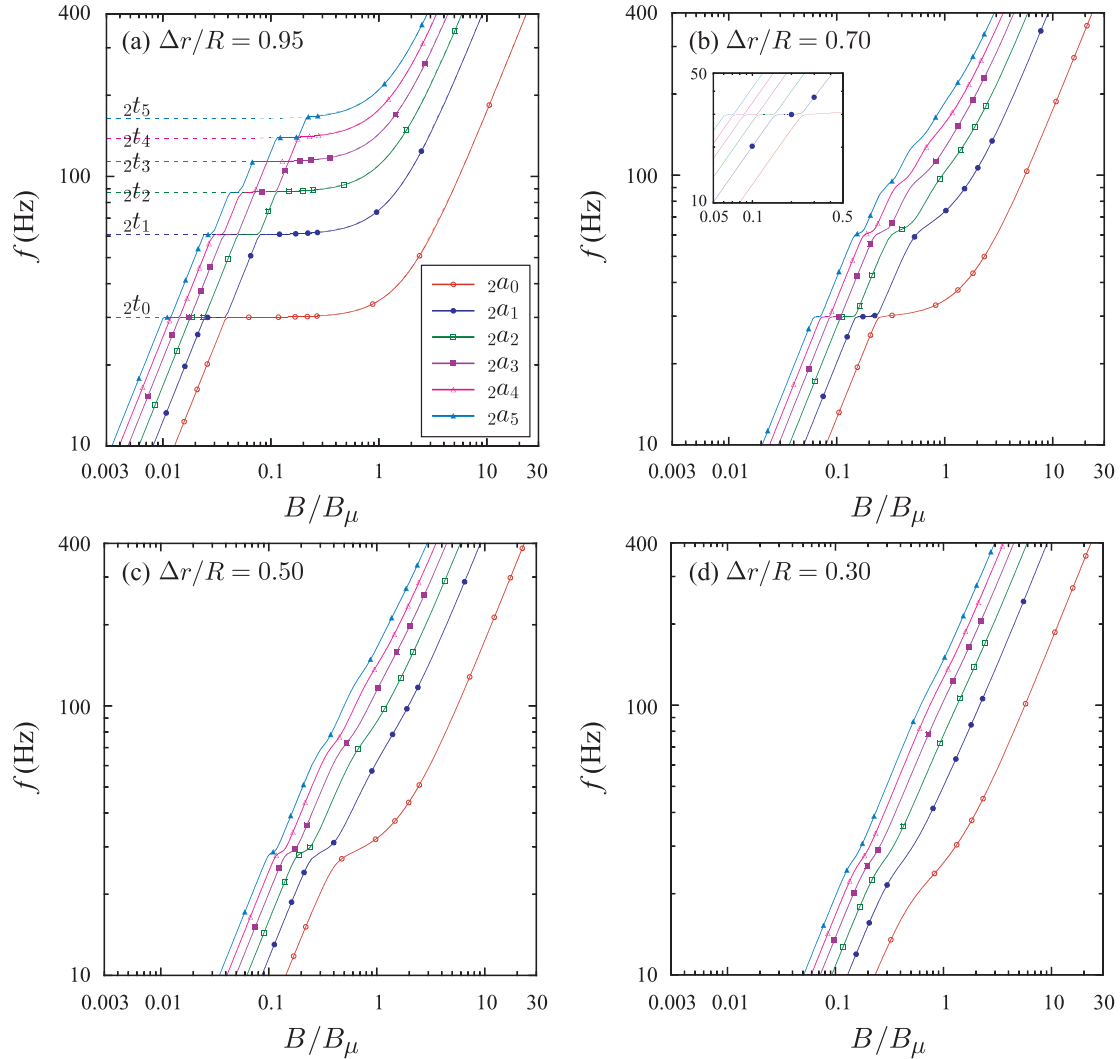


Figure 4. The behavior of torsional crust modes (${}_2t_n$) and global Alfvén modes (${}_2a_n$) for different toy models, when varying the crust thickness $\Delta r/R$. The first six eigenfrequencies for $\ell = 2$ are shown. For comparison, we also plot the case of $\Delta r/R = 1.0$ (no fluid region) as dashed lines in panel (a).

the continuous sequence changes into fundamental Alfvén mode, ${}_2a_0$, (third filled circle at $B/B_\mu = 0.3$). Figure 5 shows that each of the above three eigenfunctions has one node. Specifically, the eigenfunctions for the ${}_2a_1$ and ${}_2t_0$ modes have one node in the fluid region while the ${}_2a_0$ mode has one node in the crust.

We further observe that the amplitude of the ${}_2a_0$ and ${}_2a_1$ Alfvén modes is larger in the fluid region, while the amplitude of the ${}_2t_0$ mode is larger in the crust region. This is consistent with the interpretation that, even with the presence of a large number of avoided crossings, horizontal branches correspond to predominantly crust-like modes, while branches of increasing frequency (with increasing magnetic field strength) correspond to predominantly Alfvén-like modes (except for the magnetically-dominated branch of crust modes). Of course, in the above example a large crust thickness of $\Delta r/R = 0.70$ was used, where the two family of modes are still distinguishable. For a much smaller crust thickness, the the horizontal branch of crust modes cannot be clearly identified (due to the strong avoided crossings), while the magnetically-dominated branch of crust modes is merged with the Alfvén modes, as both families of modes have nearly the same frequencies and slopes at large magnetic field strengths.

3.3 Global Alfvén modes for realistic models

Realistic stellar models have very thin solid crusts and the frequency spectrum of global modes approaches that of the pure Alfvén modes. As an example, Figure 6 shows the three lowest-order $\ell = 2$ modes, ${}_2a_0$, ${}_2a_1$, and ${}_2a_2$ for model A+DH₁₄. Pure Alfvén modes (no solid crust) are shown as solid lines while the modes in the presence of the crust are shown as dashed

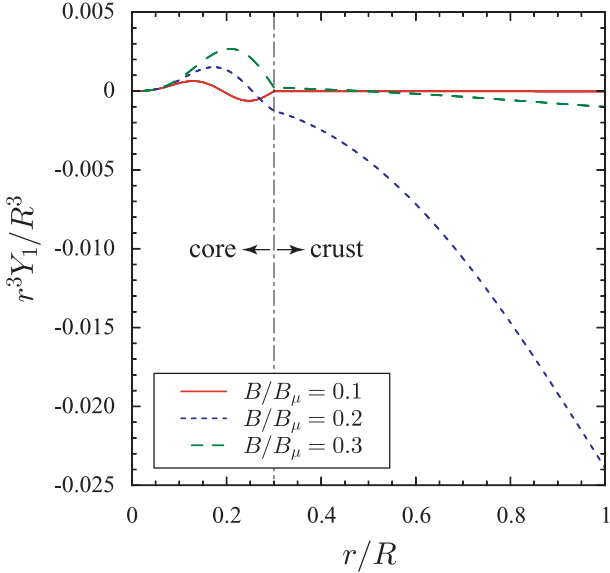


Figure 5. Scaled eigenfunctions of the $2a_1$ (at $B/B_\mu = 0.1$), $2t_0$ (at $B/B_\mu = 0.2$) and $2a_0$ (at $B/B_\mu = 0.1$) modes for a toy model with large crust thickness of $\Delta r/R = 0.70$. The number of nodes and the relative amplitude at the crust/fluid regions is consistent with the expected behavior for predominantly crustal modes and predominantly Alfvén-like modes, respectively.

lines. The pure crustal fundamental mode (when the magnetic field is confined to the crust region only, see Paper I) is also shown as a dash-dotted line. For weak magnetic fields the presence of the solid crust has some effect on the Alfvén mode frequencies, but, for large magnetic fields the effect diminishes. For larger ℓ , the effect of the presence of a solid crust on the mode frequencies persists for somewhat stronger magnetic fields.

Since the global modes for large magnetic field strengths are almost identical to pure Alfvén modes, Equation (17) describes their frequencies with good accuracy, for large magnetic field strengths. In addition, the non-degeneracy of the frequency of overtones for different values of the harmonic index ℓ will be important in trying to match numerical results to observed frequencies.

4 COMPARISON WITH OBSERVED FREQUENCIES IN SGRS

As mentioned in Paper I, it is difficult to explain all of the observed frequencies in SGRs using pure crustal torsional modes (with magnetic fields confined to the crust only). An example is the small separation of the two frequencies of 26 and 29 Hz for SGR 1806-20. Here, we find that such frequency data can be easily explained with global Alfvén modes, owing to the non-degeneracy of overtones for different values of ℓ .

Figure 7 shows, as an example, various global Alfvén mode frequencies for model A+DH₁₄. In this figure, the horizontal broken lines denote the observational data up to 150 Hz for SGR 1806-20 while the solid lines denote our computed frequencies. We find an excellent agreement between observed and computed frequencies for a magnetic field strength of $B/B_\mu \approx 1.25$, (shown as a vertical dash-dotted line). Specifically, the observed frequencies of 18, 26, 29, 92.5, and 150 Hz can be identified with the $2a_0$, $4a_0$, $5a_0$, $5a_2$, and $5a_4$ modes, respectively.

Figure 8 shows a similar excellent agreement of the observed frequencies for SGR 1900+14, with the frequencies of the $2a_0$, $7a_0$, $3a_1$, and $6a_2$, respectively, for the same chosen stellar model A+DH₁₄ and a slightly larger magnetic field strength. Since the global frequencies are sensitive to both the stellar parameters and the magnetic field strength, an independent determination of the compactness of the star would allow for a determination of the magnetic field.

The higher-frequency observational data for SGR 1806-20, such as 626.5, 720, 1837, and 2384 Hz could be also be identified with higher overtones of global Alfvén modes, as there exist many higher overtones with different ℓ . For example, for model A+DH₁₄ and with $B/B_\mu = 1.25$ (as above), we compute the following mode frequencies: $4a_{25} = 632$, $4a_{29} = 724$, $2a_{83} = 1841$, and $2a_{108} = 2382$ Hz, which are in all good agreement with the observed frequencies. We remark that both the 626.5 and 720 Hz frequencies can be identified with some global Alfvén modes, while this would not be possible with the crustal modes, when the magnetic field is confined to the crust (see numerical results in Paper I), due to the near degeneracy of overtones of different ℓ .

Table 4 shows the maximum values of the magnetic field, for which one can at least identify the frequency of the $2a_0$ mode. For models which have no entry in this Table, such an identification was not possible. In reality, some stellar models with lower magnetic strength can agree well with the observational data, if the $2a_0$ mode is omitted. For example, the stellar

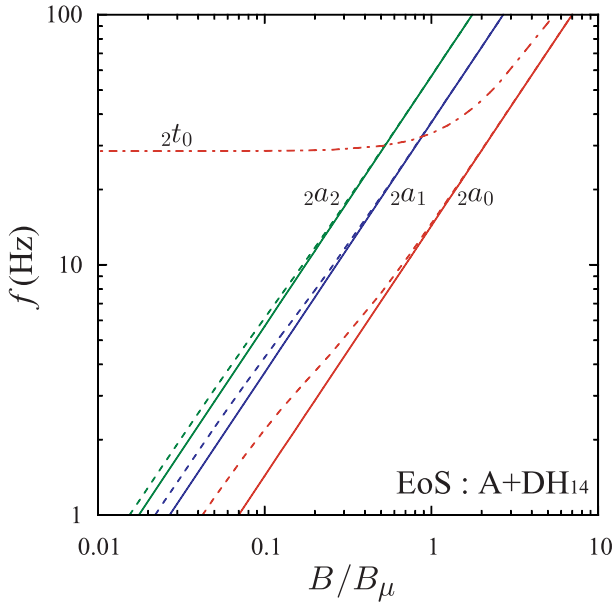


Figure 6. The frequencies of global Alfvén modes ${}_{\ell}a_n$ with $\ell = 2$ and $n = 0, 1,$ and 2 as functions of the normalized magnetic field (B/B_μ). The dashed line corresponds to a realistic model (A+DH₁₄) with both fluid and solid regions. The solid line corresponds the same model, but setting $\mu = 0$ in the crust region (pure magneto-fluid). The differences between the two cases are limited to small magnetic field strengths, while for higher values there is coincidence. For comparison, we also show the ${}_{2}t_0$ pure crustal mode (when the magnetic field is confined to the crust).

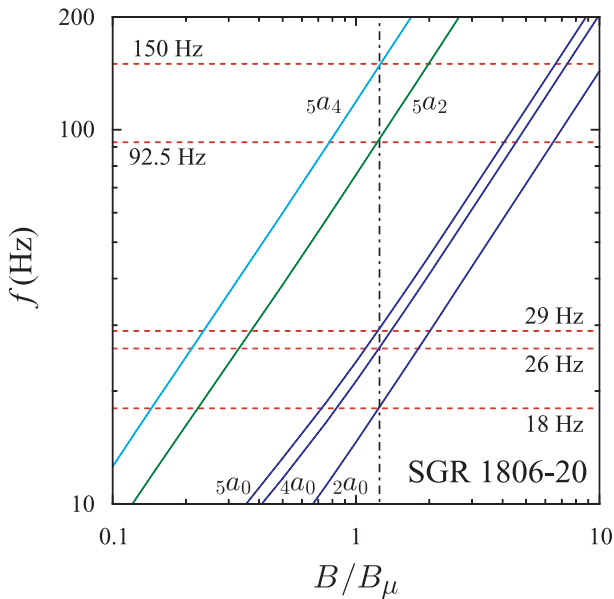


Figure 7. Comparison of several specific Alfvén modes (solid lines) with observed frequencies for SGR 1806-20 (horizontal dashed lines) for the stellar model A+DH₁₄. The agreement for all frequencies up to 150 Hz is excellent, for a magnetic field strength of $B/B_\mu \approx 1.25$ (vertical dashed-dotted line).

model with L+NV₁₈ and $B/B_\mu = 0.60$ can agree well with all observational data lower than 150 Hz, when identified with the frequencies of the ${}_{4}a_0$, ${}_{8}a_0$, ${}_{10}a_0$, ${}_{2}a_6$, and ${}_{2}a_{11}$ modes respectively. As seen Figure 3 there are no global Alfvén modes with frequency less than that of the ${}_{2}a_0$ mode. Thus, the values in Table 4 correspond to the maximum magnetic field strength for each stellar model, if the observational data could be explained by the global Alfvén modes. The maximum magnetic field strength is $B/B_\mu \approx 2$ for SGR 1806-20 and $B/B_\mu \approx 3$ for SGR 1900+14.

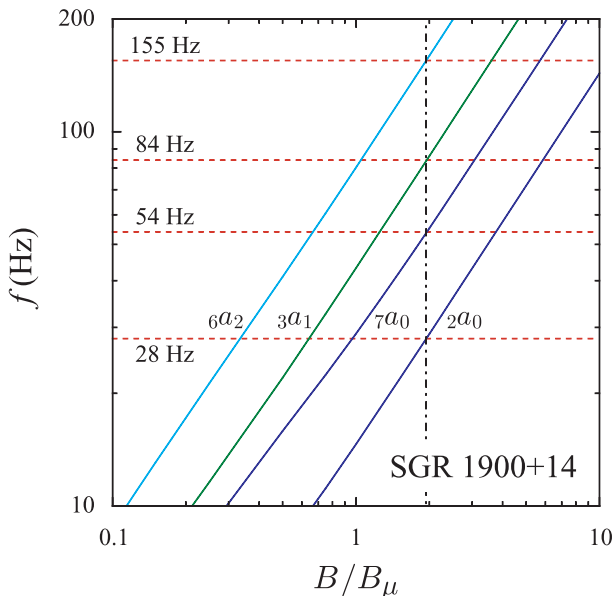


Figure 8. Comparison of several specific Alfvén modes (solid lines) with observed frequencies for SGR 1900+14 (horizontal dashed lines) for the stellar model A+DH₁₄. The agreement for all frequencies up to 150 Hz is excellent, for a magnetic field strength of $B/B_\mu \approx 1.94$ (vertical dashed-dotted line).

5 SUMMARY AND DISCUSSION

We have investigated torsional Alfvén modes of relativistic stars with a global dipole magnetic field. It has been noted recently (Glampedakis et al. 2006) that such oscillation modes could serve as an alternative explanation (in contrast to torsional crustal modes) for the SGR phenomenon, if the magnetic field is not confined to the crust. We compute global Alfvén modes for a representative sample of equations of state and magnetar masses, in the ideal MHD approximation and ignoring $\ell \pm 2$ terms in the eigenfunction. The presence of a realistic crust has a negligible effect on Alfvén modes for $B > 4 \times 10^{15}$ G. Using a toy model with large crust thickness we demonstrate that strong avoided crossings between torsional Alfvén modes and torsional crust modes take place. For magnetar-like magnetic field strengths, the spacing between consecutive Alfvén modes is of the same order as the gap of avoided crossings. As a result, it is not possible to identify modes of predominantly crustal character and all oscillations are predominantly Alfvén-like.

The Alfvén-like character of global modes allows for a non-degeneracy of overtones with different ℓ . Using this fact, we find excellent agreement between our computed frequencies and observed frequencies in two SGRs, for reasonable magnetic field strengths. We construct an empirical formula which describes the frequency of the fundamental torsional Alfvén modes (for different ℓ) as a function of the magnetic field strength and the compactness of the star. Such formulae could be used for inferring the stellar properties and magnetic field strength. The requirement that the lowest observed frequency is identified with the fundamental $2a_0$ mode leads to a maximum magnetic field strength in the range of $(0.8\text{--}1.2) \times 10^{16}$ G.

In the present work we have ignored couplings to $\ell \pm 2$ terms. A two-dimensional treatment of the eigenvalue problem will appear elsewhere.

ACKNOWLEDGMENTS

This work was supported by the Marie-Curie grant MIF1-CT-2005-021979, the Pythagoras II program of GSRT and the EU network ILIAS.

REFERENCES

- Akmal A., Pandharipande V.R., Ravenhall D.G., 1998, Phys. Rev. C 58, 1804
- Carroll B.W., Zweibel E.G., Hansen C., McDermot P.N., Savedoff M.P., Thomas J.H., Van Horn H.M., 1986, ApJ, 305, 767
- Douchin F., Haensel P., 2001, A& A, 380, 151
- Duncan R.C., Thompson C., 1992, ApJ, 392, L9
- Duncan R.C., 1998, ApJ, 1998, 498, L45
- Glampedakis K., Samuelsson L., Andersson N., 2006, MNRAS, 371, L74

Table 4. Maximum magnetic field strength, for various equilibrium models, for which the lowest frequency observed in two different SGR sources can be identified with the fundamental $2a_0$ mode.

Model	SGR1806-20	SGR1900+14
A+DH ₁₄	1.25	1.94
A+DH ₁₆	1.65	2.64
WFF3+DH ₁₄	1.04	1.65
WFF3+DH ₁₆	1.26	2.00
WFF3+DH ₁₈	1.67	2.68
APR+DH ₁₄	0.89	1.43
APR+DH ₁₆	1.07	1.69
APR+DH ₁₈	1.28	2.00
APR+DH ₂₀	1.52	2.36
APR+DH ₂₂	1.84	2.93
L+DH ₁₄	—	1.20
L+DH ₁₆	0.87	1.38
L+DH ₁₈	1.00	1.58
L+DH ₂₀	1.15	1.82
L+DH ₂₂	1.32	2.05
L+DH ₂₄	1.52	2.39
L+DH ₂₆	1.80	2.85
A+NV ₁₄	—	1.92
A+NV ₁₆	1.63	—
WFF3+NV ₁₄	—	1.58
WFF3+NV ₁₆	1.21	2.00
WFF3+NV ₁₈	1.65	—
APR+NV ₁₄	—	—
APR+NV ₁₆	—	1.70
APR+NV ₁₈	1.25	2.00
APR+NV ₂₀	1.51	2.42
APR+NV ₂₂	1.85	2.98
L+NV ₁₄	—	—
L+NV ₁₆	—	—
L+NV ₁₈	—	1.69
L+NV ₂₀	—	1.94
L+NV ₂₂	1.39	2.24
L+NV ₂₄	1.63	2.58
L+NV ₂₆	1.92	—

Hansen C., Cioffi D.F, 1980, ApJ, 238, 740
 Konno K., Obata T., Kojima Y., 1999, A&A, 352, 211
 Lee, U., 2006, astro-ph/0610182
 Leins M., 1994, PhD Thesis, University of Tübingen
 McDermott P.N., Van Horn H.M., Hansen C.J., 1988, ApJ, 325, 725
 Messios N., Papadopoulos D.B., Stergioulas N., 2001, MNRAS, 328, 1161
 Negele J.W., Vautherin D., 1973, Nucl. Phys., A207, 298
 Pandharipande V.R., 1971, Nucl. Phys. A, 178, 123
 Pandharipande V.R., Smith R.A., 1975, Phys. Lett. 59B, 15
 Piro A.L., 2005, ApJ, 634, L153
 Samuelsson L., Andersson N., preprint astro-ph/0609265
 Schumaker B.L., Thorne K.S., 1983, MNRAS, 203, 457
 Sotani H., Kokkotas K.D., Stergioulas N., 2006, MNRAS, ???, ??? (Paper I)
 Strohmayer T.E., 1991, ApJ, 372, 591
 Strohmayer T.E., Watts A.L., 2006, ApJ, in press (astro-ph/0608463)
 Wasserman I., Shapiro S.L., 1983, ApJ, 265, 1036
 Watts A.L., Strohmayer T.E., 2006, ApJ, 637, L117
 Wiringa R.B., Fiks V., Farbrocini A., 1988, Phys. Rev. C 38, 1010